NANO LETTERS

pubs.acs.org/NanoLett Letter

Atomic Scale Dynamics Drive Brain-like Avalanches in Percolating Nanostructured Networks

Matthew D. Pike,[‖] Saurabh K. Bose,[‖] Joshua B. Mallinson, Susant K. Acharya, Shota Shirai, Edoardo Galli, Stephen J. Weddell, Philip J. Bones, Matthew D. Arnold, and Simon A. Brown*

Cite This: https://dx.doi.org/10.1021/acs.nanolett.0c01096 Read Online

ACCESS | Metrics & More | Article Recommendations | Supporting Information

ABSTRACT: Self-assembled networks of nanoparticles and nanowires have recently emerged as promising systems for brain-like computation. Here, we focus on percolating networks of nanoparticles which exhibit brain-like dynamics. We use a combination of experiments and simulations to show that the brain-like network dynamics emerge from atomic-scale switching dynamics inside tunnel gaps that are distributed throughout the network. The atomic-scale dynamics emulate leaky integrate and fire (LIF) mechanisms in biological neurons, leading to the generation of critical avalanches of signals. These avalanches are quantitatively the same as those observed in cortical tissue and are signatures of the correlations that are required for computation. We show that the avalanches are associated with dynamical restructuring of the networks which self-tune to balanced states consistent with self-organized criticality. Our simulations allow visualization of the network states and detailed mechanisms of signal propagation.

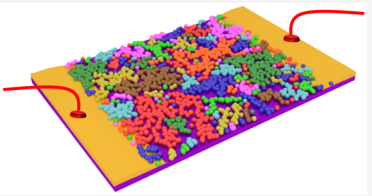

KEYWORDS: *Brain-like networks, percolation, scale-free dynamics, long-range temporal correlations, criticality, nanoparticle networks, neuromorphic computing*

Neuromorphic, or brain-like, computing is motivated both by the recognition that traditional integrated circuit technologies are reaching fundamental limits[1,2] and by the remarkable capability of the biological brain to perform tasks such as pattern recognition in an extremely energy-efficient way.[3−5] A wide variety of brain-inspired approaches to computing are being investigated, using, for example, CMOS neurons and synapses,[6,7] memristors,[8−10] atomic switches,[11,12] and phase change materials,[13] but there have been relatively few attempts to develop intrinsically brain-like architectures which might support neuromorphic computing in a more natural way than standard (highly organized) chip architectures.

Motivated by calculations which show that optimal information processing is achieved by intrinsically complex architectures operating at criticality[14,15] and that scale-free, hierarchical networks are valuable[16] in enhancing neuromorphic approaches such as reservoir computing (RC),[5,17,18] several groups have begun to explore the properties of self-assembled nanoscale networks.[19,20] This approach was initially driven by investigations of networks of silver nanowires,[12,21] which exhibit interesting dynamics and were used in first attempts to perform waveform regression tasks.[22] More recently other nanowire systems have been investigated,[23,24] and it has emerged that percolating-tunneling networks of nanoparticles also exhibit complex dynamics,[25−28] brain-like avalanches and criticality,[29] and long-range temporal correlations (LRTCs) due to their intrinsically scale-free network architectures.[30]

In this Letter we show that brain-like network dynamics in percolating networks of nanoparticles emerge from atomic scale dynamics inside tunnel junctions within the networks. We first present experimental data that reveals the atomic scale dynamics and show that they emulate some of the functions of biological neurons. We then use computer simulations to demonstrate that, when coupled with the underlying scale-free network architecture,[30] these dynamics lead to critical avalanches of signals that are similar to those observed experimentally and which, in turn, are quantitatively the same as those observed in cortical tissue.[15,31] We show that criticality emerges only in a parameter range where the network self-tunes to a state with an optimal number of pathways through the network, consistent with self-organized criticality.[32] Finally, by comparing the experimental and simulational results, we show that the distribution of measured changes in conductance reflects the dynamical structure of the network and for the first time demonstrate the detailed mechanism for the propagation of critical avalanches in self-assembled networks.

Our percolating networks of nanoparticles are formed through deposition of nanoparticles onto silicon nitride

Received: March 11, 2020
Revised: April 27, 2020
Published: April 29, 2020

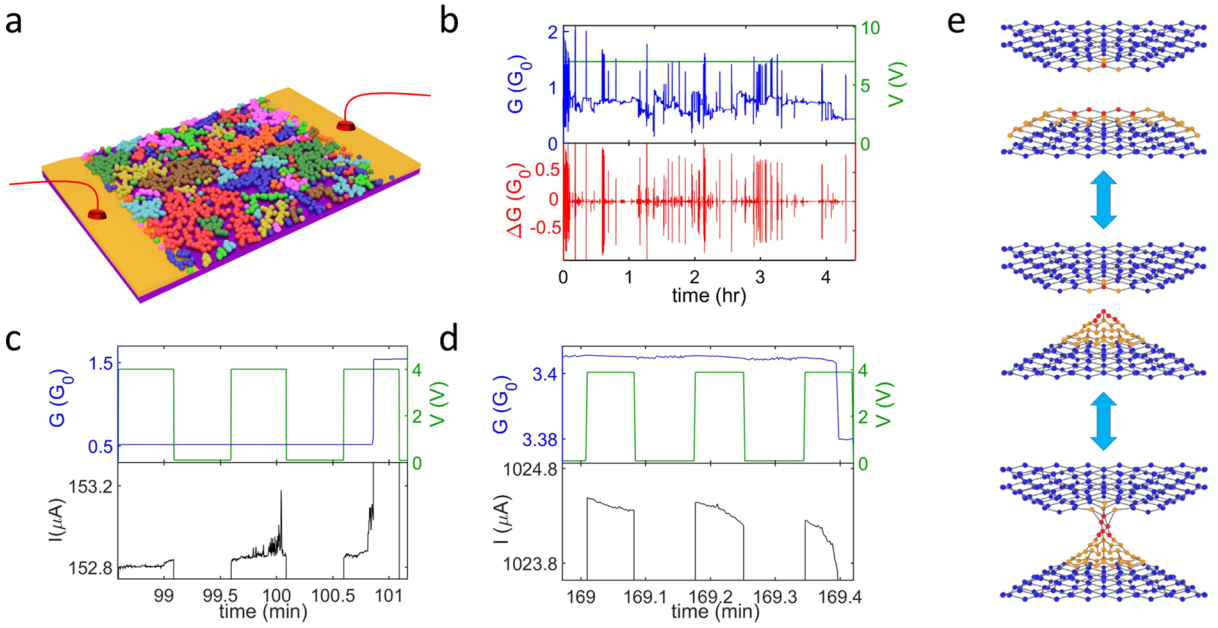

Figure 1. Atomic-scale dynamics in percolating nanoparticle networks. (a) Schematic illustrating two-terminal device geometry with the interconnected nanoparticle groups (different colors) separated via tunnel gaps. (b) Representative conductance data, measured over many hours with 100 ms sampling interval (see Methods), showing complex patterns of switching events and bursty dynamics.[29,30] Voltage stimulus (green), device conductance (G, blue, in units of $G_0 = 2e^2/h$, the quantum of conductance), and event size (ΔG, red). (c) Low-voltage pulsed stimulus, focusing on a single switching event (time-window 2.5 min), reveals clear signatures of signal integration prior to "firing", corresponding to electric field induced atomic hillock formation. (d) Electromigration-induced reverse process reduces the average width of a pre-existing atomic filament (decreasing I), eventually resulting in filament-breaking. (e) Schematic of atomic-filament formation/destruction process.[33−35]

substrates.[25,26] Deposition is terminated when the fraction (p) of the surface area covered with conducting particles approaches the percolation threshold ($p_c \sim 68\%$), which is a critical value separating the insulating and the conducting states.[36] Figure 1a shows a schematic of our two electrode devices. During deposition (see Methods), particles come into contact and form interconnected groups which are separated by tunnel gaps (which have a distribution of sizes[37]) and which have varying sizes and fractal geometries.[30] Groups are collections of particles that are in Ohmic contact with one another. We emphasize that after deposition the overall structure of the network is fixed, in contrast to many other devices (see, e.g., ref 38) where memristive behavior results from significant rearrangements of nanoparticles. This distinction is illustrated in Figures S6 and S7.

The tunnel gaps act as switching sites; upon application of an external voltage stimulus, atomic scale filaments can be formed (and subsequently broken) in the tunnel gaps,[25] resulting in changes in the network conductance (G) shown in Figure 1b. These switching events occur in bursts, or avalanches, that have been shown to exhibit[29] the same statistical properties as avalanches of neuronal signals in the cortex,[31] thus demonstrating the strong spatiotemporal correlations required for RC and strong potential for optimal information processing[39] (see refs 29 and 30 for further details).

The atomic scale switching processes that cause correlations and avalanches are yet to be studied in percolating networks, because most switching events occur on time scales[11] that are far quicker than can be recorded by the measurement system. Here, using low-voltage pulsed stimulation, we have interrogated the switching processes and resolved for the first time the dynamics of some switching events. Figure 1c,d shows portions of experimental conductance traces, which capture formation (Figure 1c) and destruction (Figure 1d) of atomic scale filaments, following the behavior shown schematically in Figure 1e and described in more detail in the next paragraph.

Figure 1c shows an initial increase in conductance as electric field induced surface diffusion (EFISD)[33,34] causes atoms on the surface of the nanoparticles to accumulate in a "hillock" (yellow in Figure 1e), decreasing the size of the tunnel gap. During the second pulse, filament formation nearly reaches completion, but because the applied electric field is close to the threshold for inducing atomic motion, fluctuations in the conductance are observed. Toward the end of the pulse, the hillock of atoms relaxes so that the conductance returns to a value near to its initial level. During the third pulse, the hillock of atoms extends completely across the tunnel gap, forming a filament (red in Figure 1e) that has relatively high conductance (of the order of the quantum of conductance, $G_0 = 2e^2/h$).[25] This switching event causes an increase in observed network conductance, as well as a reduction of the potential difference between the two groups of nanoparticles. Figure 1d shows the reverse process, i.e., over three voltage pulses electromigration effects[35] reduce the average width of a previously formed filament until it is broken, causing a clear decrease in the network conductance.

An important feature of these results is that the effect of the applied electric field/current is cumulative, i.e., both formation and destruction of the atomic scale filaments can be viewed as integrating the applied signals until filament formation/destruction ("firing"). The fluctuations[40] in Figure 1c are consistent with surface energy effects,[41] which attempt to return the gap/filament to its original size ("leak") when there is no current/voltage. As is shown in more detail in Figure S1, these processes are therefore qualitatively similar to leaky

https://dx.doi.org/10.1021/acs.nanolett.0c01096
Nano Lett. XXXX, XXX, XXX−XXX

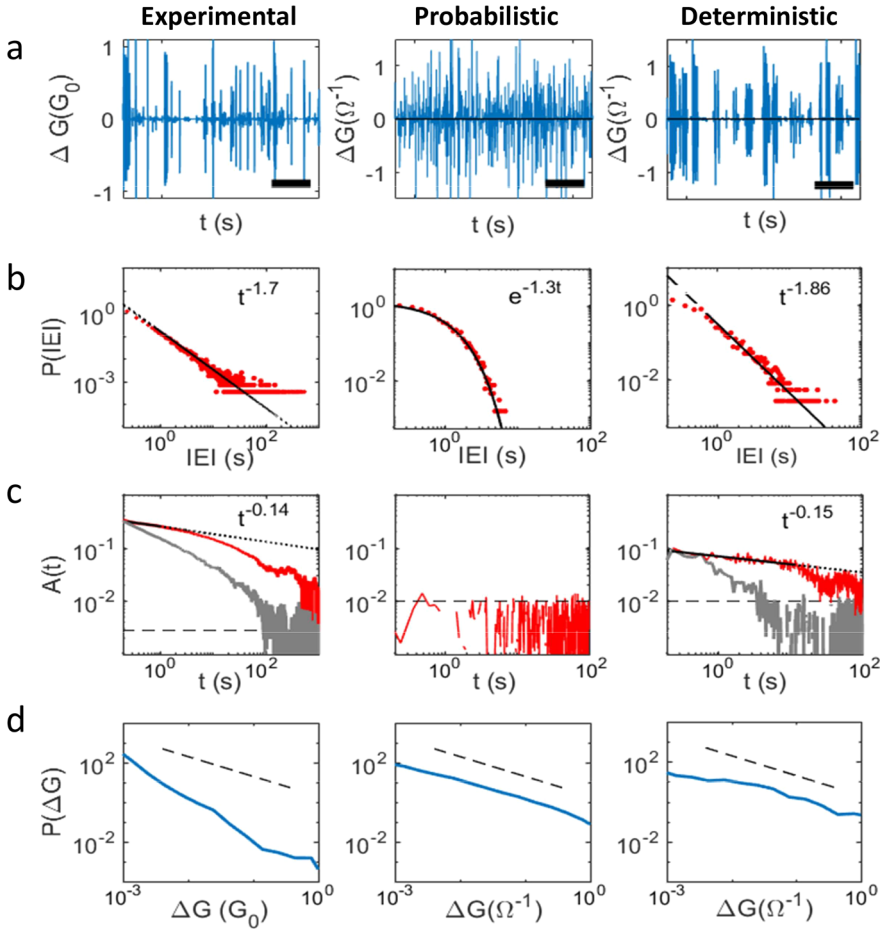

Figure 2. Switching dynamics in the experiments (left column), probabilistic-model (center column), and deterministic model (right column). (a) Experimentally observed bursty behavior is reproduced by the deterministic model but is absent in the probabilistic model (scale bar = 2000*s*). (b) The distribution of interevent intervals (P(IEI)) is a power law for the experimental data and the deterministic model (with a similar slope) but decays exponentially for the probabilistic model (black: maximum likelihood fit). (c) Autocorrelation function $A(t)$ (red) is a power law for both experimental data and deterministic model with $t^{-0.14}$ but is essentially zero (i.e., below the confidence bound (dashed lines)) for the probabilistic model. Shuffling the IEI sequence (gray) leads to a lower $A(t)$ (see refs 29 and 30 and refs therein). (d) Distribution of event sizes (P(ΔG), blue) exhibits a heavy-tail in all cases. The black dashed line (slope = −1) is a guide to the eye. The slopes in the simulations are smaller (by a factor of 2) than observed experimentally due to the smaller system size in the simulations.

integration and fire (LIF) mechanisms in biological neurons.[42,43]

We now show, using computer simulations, that when coupled with the intrinsically scale-free architecture of the percolating-tunneling network,[30] this local integrate and fire (IF) mechanism leads to long-range temporal correlations and the generation of the avalanches of events that are very similar to those observed experimentally. [Note that detailed modeling of the atomic scale processes that lead to the LIF dynamics is potentially very interesting but would require significant extensions of the models of refs 33, 34, and 38.] The experimental results are summarized in the left columns of Figures 2 and 3, see captions and Methods for details. The essential points are (i) distributions of interevent intervals (IEIs) and the autocorrelation functions (ACFs) in Figure 2 are power laws, which are characteristic of long-range temporal correlations (LRTC),[30] and (ii) the power law avalanche distributions in Figure 3 are consistent with criticality.[29,44] The heavy-tailed ΔG distributions (Figure 2d) reflect the dynamical nature of the network, as discussed below.

Numerical simulations have been used previously to show that the experimental networks of nanoparticles are well described by continuum models[37,45] in which the conducting objects are represented by uniform discs, which are allowed to overlap, representing formation of groups of particles.[37,46] Below the percolation threshold ($p < p_c$), no single group spans the entire network and the conduction of the system is due to the tunnel currents flowing across small tunnel gaps which separate the groups of particles. It is assumed that the groups are large enough that both the charging energy of a connected group and the quantization of energy levels are negligible and that the resistance between overlapping particles within a group is negligible, so that the only resistance in the system is due to the tunnel gaps. Each gap is assigned a conductance, $G_i = A \exp(-\delta L_i)$, where A and δ are constants and L_i is the size of the gap (in units of the particle diameter which is set to 1; $A = 1\ \Omega^{-1}$ and $\delta = 100$ for convenience).[37] After the formation of a filament, the gap is assigned a conductance $G = 10\ \Omega^{-1}$; the precise conductance values are not important and could be scaled to match the experiments more closely, but we choose to maintain consistency with previous work.[37] We focus primarily on simulations of systems with a size of $L \times L$ particle diameters ($L = 200$ is chosen to provide the best trade-off between computational time and

https://dx.doi.org/10.1021/acs.nanolett.0c01096
Nano Lett. XXXX, XXX, XXX−XXX

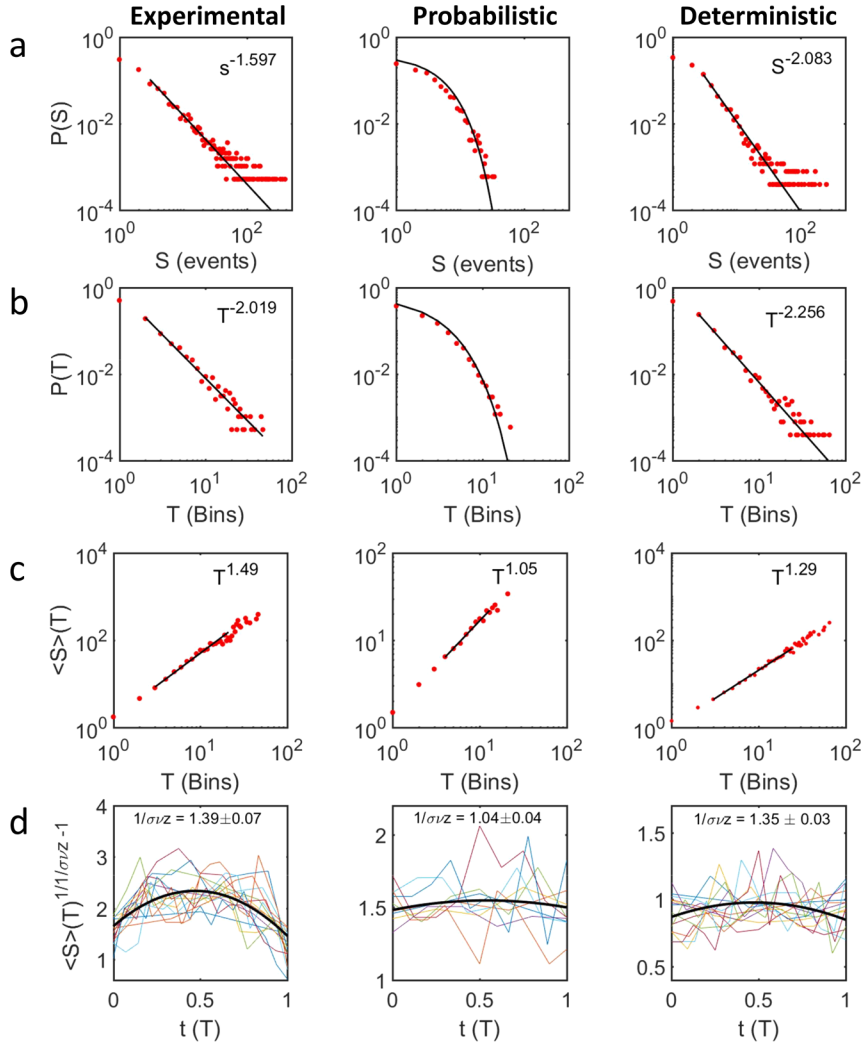

Figure 3. Avalanche and criticality analysis for the experimental data (left column), probabilistic model (center column), and deterministic model (right column). (a and b) Sizes (S) and durations (T) of the avalanches are distributed as power laws for the experimental data and the deterministic model, with slopes that are the same to within $\lesssim$20%, but the probabilistic model results in exponential distributions (black: maximum likelihood fit). (c) Average avalanche size for given duration $\langle S\rangle$ (T) $\sim T^{1/\sigma\nu z}$ with exponent $1/\sigma\nu z \sim 1.3-1.5$ for experimental data and deterministic model (a difference of only ~10%), whereas the probabilistic model yields $1/\sigma\nu z \sim 1$. (d) Average avalanche shapes for each duration showing collapse onto a universal scaling function (black line), and yield independent measures of the critical exponent $1/\sigma\nu z$. The power law behavior and agreement of estimates of $1/\sigma\nu z$ for the experimental data and deterministic model are consistent with criticality.[29,44] See also Table 1.

finite-size effects) and surface coverage $p < p_c$, but the results are substantially the same for $0.64 \leq p < p_c$ and for $200 \leq L \leq 400$, consistent with ref 30.

We first consider a probabilistic model.[46] When the electric field in a gap or the current in a filament is greater than a threshold value, the switch is allowed to change state (switch on (↑) or off (↓)) with a well-defined probability (here, $p_\uparrow = p_\downarrow = 0.001$, but the results are qualitatively independent of the parameter values). This model allows demonstration of interesting switching behavior (and in particular the formation of connected pathways across the network[46]), as well as consequent redistribution of voltages and currents through the network. However, the results in the center column in Figure 2(b, c) show that the IEI distribution is exponential (not power law, as in the experiments), and the corresponding ACF shows an absence of correlations. Similarly, the center column of Figure 3(a, b) shows that the distributions of avalanche sizes (S) and durations (T) are exponential. The absence of correlations is not surprising; in the probabilistic model the switching events occur randomly, so there is no possibility that correlated avalanches can emerge.

We now consider a new deterministic model which captures the atomic scale dynamics of the switching process described in Figure 1. To emulate the experimentally observed behaviors, the size of each tunnel gap (d_i) changes in response to the electric field E_i in the gap according to

$$\Delta d_i = \begin{cases} r_d(E_i - E_T), & \text{if } E_i \geq E_T \\ 0, & \text{otherwise} \end{cases} \quad (1)$$

and the current flow (I_j) in each existing filament causes electromigration effects[35] that decrease its width (w_j) according to

$$\Delta w_j = \begin{cases} r_w(I_j - I_T), & \text{if} I_j \geq I_T \\ 0, & \text{otherwise} \end{cases} \quad (2)$$

https://dx.doi.org/10.1021/acs.nanolett.0c01096
Nano Lett. XXXX, XXX, XXX−XXX

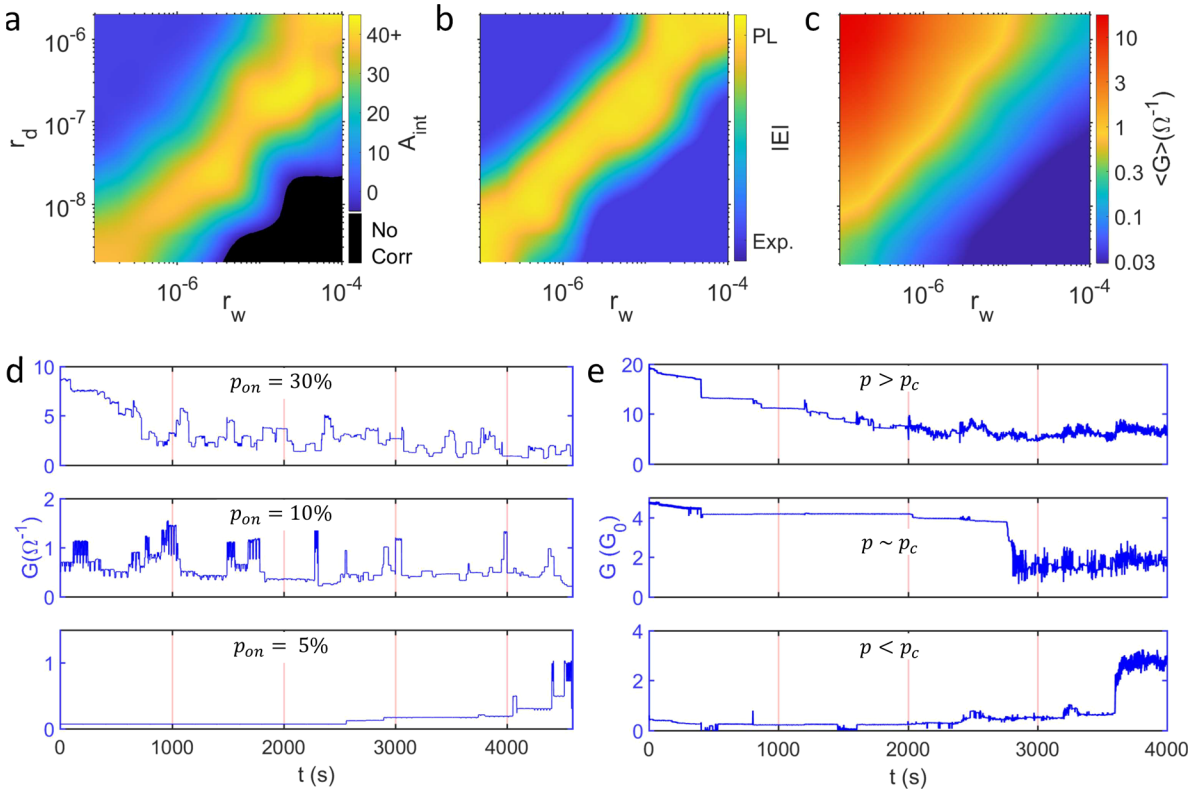

Figure 4. Maps of parameter space (r_d, r_w; see eqs 1 and 2) for the deterministic model showing a self-tuned critical state. (a) Strength of correlations (integrated autocorrelation A_{int}; see Methods) and (b) characterization of the power law (PL) and exponential (Exp.) fits to the IEI distribution. Both (a) and (b) show a clear ridge ($r_d \sim r_w/25$) corresponding to strong correlations and criticality. (c) Average network conductance showing that the ridge in parameter space corresponds to $\langle G \rangle \sim 0.5\ \Omega^{-1}$. Note that the parameters chosen to illustrate the deterministic simulations in Figures 2 and 3 correspond to a point on this ridge ($r_d = 5 \times 10^{-7}\ V^{-1}$, $r_w = 3 \times 10^{-5}\ A^{-1}$). (d) Initial states in which 5%, 10%, and 30% of switches are "on" all self-tune toward $G \sim 0.5\ \Omega^{-1}$. (e) Corresponding experimental data showing that under voltage stimulus devices with different surface coverages self-tune toward critical states with $1 \lesssim G \lesssim 6G_0$. The difference between optimum values of G in the experiment and simulation results from the choice of simulation parameters, which maintains consistency with previous work.[37]

where r_d and r_w are parameters that control the rates at which d and w change when threshold fields (E_T) and currents (I_T), respectively, are exceeded. Here, E_T = 10 V and I_T = 0.01A, which are chosen to be consistent with estimates obtained from experiments.[25]

The right column in Figure 2(b, c) shows that the deterministic model reproduces the power law IEI distribution and strong correlations observed in the experiments. The right column in Figure 3(a, b) shows that the deterministic model also reproduces the power law distributions of S and T. Furthermore, for the deterministic simulations, the three different estimates of the critical parameter $1/\sigma\nu z$ shown in Table 1 are in good agreement, therefore satisfying rigorous criteria for criticality.[29,31,44] The deterministic simulations are in excellent qualitative agreement with the experiments for a broad range of parameters (see below), while the probabilistic simulations fail to reproduce the observed power law behavior. The already good quantitative agreement between the deterministic simulations and the experiments in Figures 2 and 3 could most likely be improved even further by fine-tuning the model parameters. The optimum simulation parameters are expected to be material dependent.

The deterministic simulations allow the generation of maps of the current and voltage distributions in the network at each time step, providing a method to elucidate the mechanism for the propagation of the critical avalanches (Figure S2 and Video V1). When an external stimulus (voltage) is applied, the formation (or annihilation) of an atomic filament at a tunnel gap redistributes current across the entire network, thereby modifying local electric fields in other tunnel gaps. This in turn changes the rates at which tunnel gaps/filaments change size (see eqs 1 and 2), leading to further switching events. In other words, each switching event influences subsequent switching events through internal feedforward and feedback, giving rise to temporal correlations. We emphasize that it is this correlated switching behavior in the deterministic simulations that leads to the critical dynamics; the absence of the correlated switching in the probabilistic case leads to noncritical dynamics.

We now turn to a discussion of the distribution of ΔG values which, as shown in Figure 2d, are heavy-tailed for both experimental and simulational data. Both the deterministic and probabilistic models generate similar distributions (Figure 2d center and right panels). The ΔG distributions for the ensemble of switches reflect both the positions of the individual switches in the network and the number of times the switches open or close.[30] Figure S3 reveals that the values of ΔG measured for individual switching sites are also distributed over several orders of magnitude. As shown in Figure S4, this surprising result is due to dynamical reconfiguration of the network; at different times each switch can find itself on different branches of the (fractal)[30] arrangement of current paths. Hence, even though the change in conductance of any individual switch is essentially the same,

https://dx.doi.org/10.1021/acs.nanolett.0c01096
Nano Lett. XXXX, XXX, XXX−XXX

Table 1. Criticality in the Experiments and Deterministic Simulations[a]

exponent	τ	α	crackling relationship	$\langle S \rangle$ (T)	shape collapse
Experimental	1.6 ± 0.1	2.0 ± 0.1	1.7 ± 0.2	1.49 ± 0.03	1.39 ± 0.07
Deterministic Simulation	2.1 ± 0.1	2.6 ± 0.1	1.2 ± 0.2	1.29 ± 0.02	1.35 ± 0.03

[a]The critical exponent $1/\sigma\nu z$ is obtained from the crackling relationship $(\alpha - 1)/(\tau - 1)$, mean avalanche size given duration $\langle S \rangle$ (T), and avalanche shape collapse for both representative experimental data and the deterministic simulations. The agreement of these three independent estimates of $1/\sigma\nu z$ is a rigorous requirement for criticality. See refs 29, 31, and 44 for details of the criticality analysis.

each time the switch changes state the configuration of the rest of the network is different so a different value of ΔG is measured.

Finally, we discuss the range of parameter space in the deterministic model in which correlations and critical avalanches are observed. Figures 4a and 4b show that strong correlations and power law IEI distributions are obtained along a diagonal ridge in the r_d, r_w parameter space. Figure 4c shows that this ridge corresponds to a narrow range of conductances, where the connectivity of the network is optimized for criticality; the number of switches in their "off" or "on" states is "balanced". The nature of the balanced state is illustrated by the results of simulations in which the initial state of the network is chosen to have different numbers of switches in the "on" state (Figure 4d). When the number of switches that are "on" is high, the resulting high current will tend to break filaments and return the system to the balanced state. Conversely, if the number of switches that are "on" is low, higher electric fields in some tunnel gaps will cause additional switches to turn "on", again returning the system to the balanced state. Hence, the system always self-tunes to a dynamical state where the number of pathways through the network is close to an optimum value. This "balance" is essential for critical avalanches to propagate.[15,39]

Figure 4e shows that the experimental system self-tunes to achieve a similar balance. If the initial conductance of the network (G_{init}, measured immediately after deposition) is either higher or lower than the narrow range $(1 \lesssim G \lesssim 6G_0)$ in which correlations and criticality are observed,[29] switches change state so as to move the system back into that G range.

In summary, we have presented experimental evidence for atomic-scale integrate and fire mechanisms within our percolating networks and shown by detailed modeling that these processes facilitate critical avalanches. Both experimental and simulational results are consistent with optimally balanced network states similar to the self-organized-critical states reported in biological neuronal networks.[47,48] These results provide a significant step toward understanding the dynamics of nanoscale switching networks, and will facilitate the development of applications. For example, as discussed in some detail in refs 29 and 30, performance of pattern recognition algorithms based on reservoir computing[5,17,18] is believed to be optimized for scale-free[16] and critical[14,15] networks, and we believe there are many new opportunities to be explored in the field of unsupervised learning.[10]

METHODS

Experimental methods and analysis have been described in detail in refs 29 and 30, so we provide here only a brief summary.

Device Fabrication. Our percolating devices are fabricated by simple nanoparticle deposition processes.[25,26,49] 7 nm Sn nanoparticles are deposited between gold electrodes (spacing 100 μm) on a silicon nitride surface and coalesce to form particles of 20 nm diameter. Deposition is terminated at the onset of conduction, which corresponds to the percolation threshold.[36,49] The deposition takes place in a controlled environment with a well-defined partial pressure of air and humidity, as described in ref 26. This process leads to controlled coalescence and fabrication of robust structures which function for many months, but which yet allow atomic scale switching processes to take place unhindered.

Electrical Stimulus and Measurement. Electrical stimuli are applied to the electrode on one side of the percolating device, while the opposite electrode of the system is held at ground potential. DC measurements over long time periods are necessary to avoid significant cut-offs in power law distributions.[50,51] Pulsed measurements are used to probe atomic scale dynamics. The conductance measurements reported here are performed with 100 ms sampling intervals, but we have shown previously[29,30] that *quantitatively* the same behavior is observed for much shorter sampling intervals.

Data Analysis. The data analysis methods used to identify avalanches of switching events are substantially the same as those developed in the neuroscience community to analyze microelectrode array recordings from biological brain tissue and that are described in detail in ref 29.

To quantify the correlations in the simulated event trains, we use the Autocorrelation Function (ACF). Since the initial values of the ACFs (commonly called "lag-1") may be affected by finite sampling rate, we use the integrated value of the ACF from $t = 0$ to 1000 s as an indicator of the correlation strength, and we use the slope of the ACF to quantify the time scale of the correlations.

Following refs 29 and 31, both in the experiments and simulations, the size (S) and duration (T) of each avalanche of signals is defined by counting the total number of events in the avalanche and the number of time bins over which the avalanche propagates. The time bins have widths corresponding to the mean IEI.

Fitting and Goodness-of-Fit. As described in detail in ref 29, we follow the maximum likelihood (ML) approach of refs 50 and 51 to estimate power law exponents in the IEI and avalanche size distributions. The ML estimators are obtained for both power law and exponential distributions. We use the Akaike information criterion[52] to identify which distribution is more likely and find in all cases that it is the power law. In all cases, we fail to reject the null hypothesis that distributions are power-law-distributed (we require p-values > 0.2), but we do reject the null hypothesis that the distributions are exponentially distributed (we find p-values < 0.01). We do not fit the event size (ΔG) distributions because the precise shape of the distributions is not important to the analysis; they are, however, well-fitted by long-tailed functions such as a weakly truncated power law.

ML methods cannot be applied to data which is not in the form of a probability distribution and so the standard linear

https://dx.doi.org/10.1021/acs.nanolett.0c01096
Nano Lett. XXXX, XXX, XXX−XXX

regression techniques are used to obtain the measured exponents for $A(t)$ and $\langle S \rangle$ (T).

■ ASSOCIATED CONTENT

Supporting Information

The Supporting Information is available free of charge at https://pubs.acs.org/doi/10.1021/acs.nanolett.0c01096.

(1) Leaky integrate and fire (LIF) mechanism due to atomic-scale dynamics; (2) simulations showing the mechanism for propagation of critical avalanches; (3) large variation of measured values of change in network conductance (ΔG); (4) dynamical reconfiguration of the network; (5) effect of additional conduction pathways on the ΔG distribution; (6) and comparison between percolating and memristive devices such as physically evolving networks; (PDF)

Avalanche propagation in the simulated network (MP4)

■ AUTHOR INFORMATION

Corresponding Author

Simon A. Brown − *The MacDiarmid Institute for Advanced Materials and Nanotechnology, School of Physical and Chemical Sciences, Te Kura Matū, University of Canterbury, Christchurch 8140, New Zealand;* orcid.org/0000-0002-6041-4331; Email: simon.brown@canterbury.ac.nz

Authors

Matthew D. Pike − *Electrical and Computer Engineering, University of Canterbury, Christchurch 8140, New Zealand*

Saurabh K. Bose − *The MacDiarmid Institute for Advanced Materials and Nanotechnology, School of Physical and Chemical Sciences, Te Kura Matū, University of Canterbury, Christchurch 8140, New Zealand;* orcid.org/0000-0001-8848-5097

Joshua B. Mallinson − *The MacDiarmid Institute for Advanced Materials and Nanotechnology, School of Physical and Chemical Sciences, Te Kura Matū, University of Canterbury, Christchurch 8140, New Zealand*

Susant K. Acharya − *The MacDiarmid Institute for Advanced Materials and Nanotechnology, School of Physical and Chemical Sciences, Te Kura Matū, University of Canterbury, Christchurch 8140, New Zealand*

Shota Shirai − *The MacDiarmid Institute for Advanced Materials and Nanotechnology, School of Physical and Chemical Sciences, Te Kura Matū, University of Canterbury, Christchurch 8140, New Zealand*

Edoardo Galli − *The MacDiarmid Institute for Advanced Materials and Nanotechnology, School of Physical and Chemical Sciences, Te Kura Matū, University of Canterbury, Christchurch 8140, New Zealand*

Stephen J. Weddell − *Electrical and Computer Engineering, University of Canterbury, Christchurch 8140, New Zealand*

Philip J. Bones − *Electrical and Computer Engineering, University of Canterbury, Christchurch 8140, New Zealand*

Matthew D. Arnold − *School of Mathematical and Physical Sciences, University of Technology Sydney, Sydney, Australia*

Complete contact information is available at: https://pubs.acs.org/10.1021/acs.nanolett.0c01096

Author Contributions

‖These authors made equal contributions.

Author Contributions

S.A.B conceived the study and initiated the project. M.D.P and S.K.B contributed equally to this work. S.K.B, J.B.M, S.K.A, E.G, and S.S performed the experiments and associated data analysis. P.J.B. and M.D.P. proposed the deterministic simulations. M.D.P and M.D.A performed the numerical simulations. S.J.W and P.J.B. helped with the numerical simulations. S.A.B., S.K.B, and M.D.P wrote the manuscript with comments from all authors.

Notes

The authors declare no competing financial interest.

■ ACKNOWLEDGMENTS

This project was financially supported by The MacDiarmid Institute for Advanced Materials and Nanotechnology, the Ministry of Business Innovation and Employment, and the Marsden Fund.

■ REFERENCES

(1) Waldrop, M. M. The chips are down for Moore's law. *Nature* **2016**, *530*, 144−147.

(2) Markov, I. L. Limits on fundamental limits to computation. *Nature* **2014**, *512*, 147−154.

(3) Bullmore, E.; Sporns, O. The economy of brain network organization. *Nat. Rev. Neurosci.* **2012**, *13*, 336−349.

(4) Wang, Z.; Wu, H.; Burr, G. W.; Hwang, C. S.; Wang, K. L.; Xia, Q.; Yang, J. J. Resistive switching materials for information processing. *Nat. Rev. Neurosci.* **2020**, *5*, 173−195.

(5) Torrejon, J.; Riou, M.; Araujo, F. A.; Tsunegi, S.; Khalsa, G.; Querlioz, D.; Bortolotti, P.; Cros, V.; Yakushiji, K.; Fukushima, A.; Kubota, H.; Yuasa, S.; Stiles, M. D.; Grollier, J. Neuromorphic computing with nanoscale spintronic oscillators. *Nature* **2017**, *547*, 428−431.

(6) Merolla, P. A.; et al. A million spiking-neuron integrated circuit with a scalable communication network and interface. *Science* **2014**, *345*, 668−673.

(7) Davies, M.; et al. Loihi: A Neuromorphic Manycore Processor with On-Chip Learning. *IEEE Micro* **2018**, *38*, 82−99.

(8) Jo, S. H.; Chang, T.; Ebong, I.; Bhadviya, B. B.; Mazumder, P.; Lu, W. Nanoscale memristor device as synapse in neuromorphic systems. *Nano Lett.* **2010**, *10*, 1297−1301.

(9) Burr, G. W.; et al. Neuromorphic computing using non-volatile memory. *Advances in Physics: X* **2017**, *2*, 89−124.

(10) Wang, Z.; et al. Fully memristive neural networks for pattern classification with unsupervised learning. *Nature Electronics* **2018**, *1*, 137−145.

(11) Terabe, K.; Hasegawa, T.; Nakayama, T.; Aono, M. Quantized conductance atomic switch. *Nature* **2005**, *433*, 47−50.

(12) Stieg, A. Z.; Avizienis, A. V.; Sillin, H. O.; Martin-Olmos, C.; Aono, M.; Gimzewski, J. K. Emergent Criticality in Complex Turing B-Type Atomic Switch Networks. *Adv. Mater.* **2012**, *24*, 286−293.

(13) Tuma, T.; Pantazi, A.; Le Gallo, M.; Sebastian, A.; Eleftheriou, E. Stochastic phase-change neurons. *Nat. Nanotechnol.* **2016**, *11*, 693−699.

(14) Srinivasa, N.; Stepp, N. D.; Cruz-Albrecht, J. Criticality as a Set-Point for Adaptive Behavior in Neuromorphic Hardware. *Front. Neurosci.* **2015**, *9*, 449.

(15) Muñoz, M. A. Colloquium: Criticality and dynamical scaling in living systems. *Rev. Mod. Phys.* **2018**, *90*, No. 031001.

(16) Deng, Z.; Zhang, Y. Collective Behavior of a Small-World Recurrent Neural System With Scale-Free Distribution. *IEEE Transactions on Neural Networks* **2007**, *18*, 1364−1375.

(17) Lukoševičius, M.; Jaeger, H. Reservoir computing approaches to recurrent neural network training. *Computer Science Review* **2009**, *3*, 127−149.

(18) Du, C.; Cai, F.; Zidan, M. A.; Ma, W.; Lee, S. H.; Lu, W. D. Reservoir computing using dynamic memristors for temporal information processing. *Nat. Commun.* **2017**, *8*, 2204.
(19) Bose, S. K.; Lawrence, C. P.; Liu, Z.; Makarenko, K. S.; van Damme, R. M. J.; Broersma, H. J.; van der Wiel, W. G. Evolution of a designless nanoparticle network into reconfigurable Boolean logic. *Nat. Nanotechnol.* **2015**, *10*, 1048−1052.
(20) Cooper, A.; Zhong, C.; Kinoshita, Y.; Morrison, R. S.; Rolandi, M.; Zhang, M. Self-assembled chitin nanofiber templates for artificial neural networks. *J. Mater. Chem.* **2012**, *22*, 3105−3109.
(21) Milano, G.; Pedretti, G.; Fretto, M.; Boarino, L.; Benfenati, F.; Ielmini, D.; Valov, I.; Ricciardi, C. Self-organizing memristive nanowire networks with structural plasticity emulate biological neuronal circuits. *arXiv* 2019; arXiv:1909.02438 (accessed Jan 15, 2020).
(22) Demis, E. C.; Aguilera, R.; Scharnhorst, K.; Aono, M.; Stieg, A. Z.; Gimzewski, J. K. Nanoarchitectonic atomic switch networks for unconventional computing. *Jpn. J. Appl. Phys.* **2016**, *55*, 1102B2.
(23) Manning, H. G.; Niosi, F.; da Rocha, C. G.; Bellew, A. T.; O'Callaghan, C.; Biswas, S.; Flowers, P. F.; Wiley, B. J.; Holmes, J. D.; Ferreira, M. S.; Boland, J. J. Emergence of winner-takes-all connectivity paths in random nanowire networks. *Nat. Commun.* **2018**, *9*, 3219.
(24) Tanaka, H.; Akai-Kasaya, M.; TermehYousefi, A.; Hong, L.; Fu, L.; Tamukoh, H.; Tanaka, D.; Asai, T.; Ogawa, T. A molecular neuromorphic network device consisting of single-walled carbon nanotubes complexed with polyoxometalate. *Nat. Commun.* **2018**, *9*, 2693.
(25) Sattar, A.; Fostner, S.; Brown, S. A. Quantized Conductance and Switching in Percolating Nanoparticle Films. *Phys. Rev. Lett.* **2013**, *111*, 136808.
(26) Bose, S. K.; Mallinson, J. B.; Gazoni, R. M.; Brown, S. A. Stable self-assembled atomic-switch networks for neuromorphic applications. *IEEE Trans. Electron Devices* **2017**, *64*, 5194−5201.
(27) Bose, S. K.; Shirai, S.; Mallinson, J. B.; Brown, S. A. Synaptic dynamics in complex self-assembled nanoparticle networks. *Faraday Discuss.* **2019**, *213*, 471−485.
(28) Minnai, C.; Bellacicca, A.; Brown, S. A.; Milani, P. Facile fabrication of complex networks of memristive devices. *Sci. Rep.* **2017**, *7*, 7955.
(29) Mallinson, J. B.; Shirai, S.; Acharya, S. K.; Bose, S. K.; Galli, E.; Brown, S. A. Avalanches and criticality in self-organized nanoscale networks. *Science Advances* **2019**, *5*, No. eaaw8438.
(30) Shirai, S.; Acharya, S. K.; Bose, S. K.; Mallinson, J. B.; Galli, E.; Pike, M. D.; Arnold, M. D.; Brown, S. A. Long-range temporal correlations in scale-free neuromorphic networks. *Network Neuroscience* **2020**, *4*, 432−447.
(31) Friedman, N.; Ito, S.; Brinkman, B. A. W.; Shimono, M.; DeVille, R. E. L.; Dahmen, K. A.; Beggs, J. M.; Butler, T. C. Universal Critical Dynamics in High Resolution Neuronal Avalanche Data. *Phys. Rev. Lett.* **2012**, *108*, 208102.
(32) Bak, P.; Tang, C.; Wiesenfeld, K. Self-organized criticality. *Phys. Rev. A: At., Mol., Opt. Phys.* **1988**, *38*, 364−374.
(33) Olsen, M.; Hummelgård, M.; Olin, H. Surface Modifications by Field Induced Diffusion. *PLoS One* **2012**, *7*, No. e30106.
(34) Onofrio, N.; Guzman, D.; Strachan, A. Atomic origin of ultrafast resistance switching in nanoscale electrometallization cells. *Nat. Mater.* **2015**, *14*, 440−446.
(35) Xiang, C.; Kim, J. Y.; Penner, R. M. Reconnectable Sub-5 nm Nanogaps in Ultralong Gold Nanowires. *Nano Lett.* **2009**, *9*, 2133−2138.
(36) Stauffer, D.; Aharony, A. *Introduction to Percolation Theory*; Taylor & Francis: 2003.
(37) Fostner, S.; Brown, R.; Carr, J.; Brown, S. A. Continuum percolation with tunneling. *Phys. Rev. B: Condens. Matter Mater. Phys.* **2014**, *89*, No. 075402.
(38) Yang, Y.; Chen, B.; Lu, W. D. Memristive Physically Evolving Networks Enabling the Emulation of Heterosynaptic Plasticity. *Adv. Mater.* **2015**, *27*, 7720−7727.
(39) Shew, W. L.; Plenz, D. The functional benefits of criticality in the cortex. *Neuroscientist* **2013**, *19*, 88−100.
(40) Barnett, R. N.; Landman, U. Cluster-derived structures and conductance fluctuations in nanowires. *Nature* **1997**, *387*, 788−791.
(41) Wang, W.; Wang, M.; Ambrosi, E.; Bricalli, A.; Laudato, M.; Sun, Z.; Chen, X.; Ielmini, D. Surface diffusion-limited lifetime of silver and copper nanofilaments in resistive switching devices. *Nat. Commun.* **2019**, *10*, 81.
(42) Burkitt, A. N. A Review of the Integrate-and-fire Neuron Model: I. Homogeneous Synaptic Input. *Biological Cybernetics* **2006**, *95*, 1−19.
(43) Gerstner, W.; Kistler, W. M.; Naud, R.; Paninski, L. *Neuronal Dynamics*; Cambridge University Press: Cambridge, 2014.
(44) Sethna, J. P.; Dahmen, K. A.; Myers, C. R. Crackling noise. *Nature* **2001**, *410*, 242−250.
(45) Grimaldi, C. Theory of percolation and tunneling regimes in nanogranular metal films. *Phys. Rev. B: Condens. Matter Mater. Phys.* **2014**, *89*, 214201.
(46) Fostner, S.; Brown, S. A. Neuromorphic behavior in percolating nanoparticle films. *Phys. Rev. E* **2015**, *92*, No. 052134.
(47) Rubinov, M.; Sporns, O.; Thivierge, J.-P.; Breakspear, M. Neurobiologically Realistic Determinants of Self-Organized Criticality in Networks of Spiking Neurons. *PLoS Comput. Biol.* **2011**, *7*, No. e1002038.
(48) Denève, S.; Machens, C. K. Efficient codes and balanced networks. *Nat. Neurosci.* **2016**, *19*, 375−382.
(49) Schmelzer, J.; Brown, S. A.; Wurl, A.; Hyslop, M.; Blaikie, R. J. Finite-Size Effects in the Conductivity of Cluster Assembled Nanostructures. *Phys. Rev. Lett.* **2002**, *88*, 226802.
(50) Clauset, A.; Shalizi, C. R.; Newman, M. E. J. Power-law distributions in empirical data. *SIAM Rev.* **2009**, *51*, 661−703.
(51) Deluca, A.; Corral, Á. Fitting and goodness-of-fit test of non-truncated and truncated power-law distributions. *Acta Geophysica* **2013**, *61*, 1351−1394.
(52) Wagenmakers, E.-J.; Farrell, S. AIC model selection using Akaike weights. *Psychonomic Bulletin & Review* **2004**, *11*, 192−196.

https://dx.doi.org/10.1021/acs.nanolett.0c01096
Nano Lett. XXXX, XXX, XXX−XXX